Atmos. Chem. Phys. Discuss., doi:10.5194/acp-2016-464, 2016
Manuscript under review for journal Atmos. Chem. Phys.
Published: 24 June 2016

Atmospheric Chemistry and Physics Discussions
Open Access

Effect of retreating sea ice on Arctic cloud cover in simulated recent global warming

Manabu Abe[1], Toru Nozawa[2], Tomoo Ogura[3], and Kumiko Takata[4,3,1]

[1] Japan Agency for Marine-Earth Science and Technology, Yokohama, Japan

[2] Okayama University, Okayama, Okayama, Japan

[3] National Institute for Environmental Studies, Tsukuba, Japan

[4] National Institute of Polar Research, Tachikawa, Japan

Correspondence to: M. Abe (abe.mnb@gmail.com)

Abstract

This study investigates the effect of sea ice reduction on Arctic cloud cover in historical simulations with the coupled Atmosphere-Ocean general circulation model MIROC5. Arctic sea ice has been shown to exhibit substantial reductions under simulated global warming conditions since the 1970s, particularly in September. This simulated reduction is consistent with satellite observation results. However, Arctic cloud cover increases significantly during October, leading to extensive reductions in sea ice because of the enhanced heat and moisture fluxes from the underlying ocean. Sensitivity experiments with the atmospheric model MIROC5 clearly show that sea ice reduction causes increased cloud cover. Increased cloud cover occurs primarily in the lower troposphere; however, clouds in the thin surface layers directly above the ocean decrease despite the increased moisture flux because the surface air

Atmos. Chem. Phys. Discuss., doi:10.5194/acp-2016-464, 2016
Manuscript under review for journal Atmos. Chem. Phys.
Published: 24 June 2016

Atmospheric Chemistry and Physics Discussions

temperature rises in these thin layers, causing the relative humidity to decrease. As cloud cover increases, the cloud radiative effect cause an increase in the surface downward longwave radiation (DLR) by approximately 40-60% compared with changes in clear-sky surface DLR in fall. These results suggest that an increase in Arctic cloud cover as a result of reduced sea ice coverage may further melt the sea ice and enhance the feedback processes of Arctic warming.

1. Introduction

Satellite observations have shown that Arctic sea ice has decreased gradually since the 1980s (Comiso et al., 2008). Recent significant reductions in Arctic sea ice occurred in 2007 and 2012. A further reduction in Arctic sea ice is likely to result from future global warming. In turn, the reduction in sea ice can accelerate surface warming in the Arctic region through various feedback processes. A major feedback process in climate change is the ice-albedo feedback, in which reduced sea ice decreases the global albedo and increases shortwave radiation entering the climate system (e.g., Manabe and Stouffer, 1980;Dickinson et al., 1987;Curry et al., 1995;Perovich et al., 2007). This feedback is likely to occur in high-latitude regions, where snow cover and sea ice are seasonally extended. Thus, the ice-albedo feedback is larger in fall, when incoming shortwave radiation in high-latitude regions is not a minimum (Yoshimori et al., 2014).

However, the reduction in sea ice also involves other feedback processes in the Arctic region (Serreze and Barry, 2011). Previous studies have suggested that extended periods of open ocean resulting from reductions in sea ice increase Arctic cloud cover and enhance Arctic amplification (e.g., Holland and Bitz, 2003;Vavrus et al., 2009;Screen and Simmonds, 2010;Serreze and Barry, 2011). With regard to recent changes in Arctic cloud cover, Schweiger (2004) reported that both satellite data from TIROS Operational Vertical Sounder (TOVS) Polar

Atmos. Chem. Phys. Discuss., doi:10.5194/acp-2016-464, 2016
Manuscript under review for journal Atmos. Chem. Phys.
Published: 24 June 2016

Atmospheric Chemistry and Physics
Discussions

Pathfinder retrievals and Advanced Very High Resolution Radiometer (AVHRR) data reveal significant decreases in cloud fractions over the Arctic sea during winter (December-January-February, DJF) and striking increases in spring (March-April-May, MAM). Wang and Key (2003) also showed an increase in the spring cloud fraction. However, the negative trend in spring cloudiness reported by Comiso (2003) is not consistent with these previous findings, suggesting uncertainty with respect to these observations. Therefore, continuous monitoring and investigation of the changes in Arctic cloudiness are required for a robust evaluation.

To monitor the change in cloudiness resulting from reduced sea ice, several recent studies have used satellite data. Liu et al. (2012) used satellite data to show that a 1% decrease in sea ice concentration leads to a 0.36-0.47% increase in cloud cover. These authors also suggested that the total variance in cloud cover from July to November can be explained by the sea ice-cloud feedback. Using satellite data, Wu and Lee (2012) showed that low autumnal cloud cover over the Beaufort Sea and East Siberian Sea increased during the period 2000-2010, especially in October. The authors suggested that the enhanced downward longwave radiation (DLR) resulting from increased cloud cover may have been responsible for the enhanced autumnal increase in the surface air temperature (SAT). In addition, the enhanced DLR can prolong the sea ice melt seasons and lead to a positive feedback involving Arctic sea ice loss.

A strong link has been identified between cloud cover variability and sea ice variability near the sea ice margins in fall using the 40-year ECMWF Re-Analysis (ERA40) data and TOVS polar Pathfinder satellite datasets (Schweiger et al., 2008). However, this previous study concluded that the radiative effect of this change is relatively small because the direct radiative effects of cloud cover changes are compensated by changes in the temperature and humidity profiles associated with varying ice conditions. A regional climate model simulation has also shown that the radiative effect of cloud cover changes is likely to be smaller than that of changes in air temperature and humidity (Rinke et al., 2013). Because of the deficiency in observed

Atmos. Chem. Phys. Discuss., doi:10.5194/acp-2016-464, 2016
Manuscript under review for journal Atmos. Chem. Phys.
Published: 24 June 2016

Atmospheric Chemistry and Physics
Discussions
Open Access

radiation data at the surface, correctly evaluating the radiative effect of cloud cover changes is difficult. Therefore, the radiative effect of cloud clover changes in the Arctic warming remains controversial.

Recent ship observations have found that cloud base heights tend to increase in September over the Arctic Ocean without sea ice cover due to heating from the ocean. This heating is enhanced because of the increased temperature gradient between the atmosphere and the ocean, weakening the stable conditions in the atmospheric boundary layer (Sato et al., 2012). This previous study indicated that convective clouds become more numerous over the Arctic Ocean. However, inconsistent results have been reported concerning the vertical profile of cloud cover changes. Whereas Kay and Gettelman (2009) showed that increased turbulent transport of heat and moisture promotes low-cloud formation, Schweiger et al. (2008) showed that low-level clouds may decrease and middle-level clouds simultaneously increase in coverage because the decreased static stability and a deepening atmospheric boundary layer contribute to a rise in the cloud level. Simulations run by Porter et al. (2012) with the Weather Research Forecasting (WRF) model support an increase in middle-level clouds in September and increases in low-level cloud cover from October to November. The vertical profile of the cloud cover change resulting from sea ice loss is under debate and may alter the evaluation of the radiative effect of cloud cover changes.

In addition to the analysis of observations, several studies have employed climate model simulations. Climate models that have simulated sea ice reduction show that Arctic cloud cover increases in fall (Vavrus et al., 2009;Vavrus et al., 2011). An increased area of open ocean enhances the heat and moisture transport from the ocean to the atmosphere, resulting in increased cloudiness. These studies have analyzed the change in cloudiness resulting from sea ice losses in simulations with increased greenhouse gas concentrations. The effects of reduced sea ice in these analyses are stronger than those occurring in the late 20th century. Therefore, these results are not always appropriate for the change in Arctic cloudiness that has occurred since the late 20th century, in which sea ice has only decreased in limited regions. These investigations may be insufficient to understand recently observed events and may not effectively explain recent processes in simulated climate models.

As noted above, several studies have investigated Arctic cloud cover changes during recent global warming. However, debate surrounds the change in Arctic cloudiness and the lack of an understanding of the effect of reduced sea ice on Arctic cloud cover because of insufficient observational data and longstanding difficulties in representing realistic polar clouds in climate models. In addition, the radiative effect of cloud cover changes at the surface is difficult to accurately measure because of the dark seasons and sea ice cover. In this study, we investigate the temporal trends of Arctic cloud cover changes during recent global warming simulated by a state-of-the-art climate model (i.e., MIROC5) and focus on the effects of reduced sea ice. The simulated vertical structure of cloud cover change is analyzed using a composite analysis technique because of continued controversy regarding the vertical profile of cloud changes. Furthermore, to provide information on the role of Arctic clouds in the mechanism of Arctic warming, this study evaluates the relative importance of changes in cloud radiative forcing on the surface DLR and those due to increased air temperature and water vapor. The Arctic cloud cover changes resulting from reduced sea ice in climate model simulations should be informative for understanding the mechanism underlying future changes in Arctic clouds and Arctic warming.

The next section explains the coupled atmosphere-ocean general circulation model (MIROC5) used in this study and its 20th century simulation. The third section reports the results for the Arctic cloud cover changes resulting from retreating sea ice. We then discuss the relationship between changes in Arctic cloud cover and sea ice changes, and the paper concludes with a summary.

Atmos. Chem. Phys. Discuss., doi:10.5194/acp-2016-464, 2016
Manuscript under review for journal Atmos. Chem. Phys.
Published: 24 June 2016

2. Model and Experiments

We analyze historical simulations using a coupled atmosphere-ocean general circulation model, i.e., MIROC5 (Watanabe et al., 2010), which was used in the Coupled Model Intercomparison Project Phase 5 (CMIP5). The atmospheric portion of MIROC5 is based on the global spectral dynamical core and includes a standard physical package. The atmospheric resolution is T85L40, with a top at 3 hPa. The ocean general circulation model in MIROC5 is the CCSR (Center for Climate System Research, University of Tokyo) Ocean Component Model (COCO) version 4.5 (Hasumi, 2007). The zonal resolution of the ocean is fixed at 1.4°, whereas the meridional resolution is 0.5° at latitudes equatorward of 8° and 1.4° at higher latitudes (poleward of 65°), with a smooth transition in between (256 × 224 grid points for the zonal and meridional directions, respectively). The model has 49 vertical levels, and the spacing varies with a depth of 2.5 m at the surface, 20 m at a depth of 100 m, 100 m at a depth of 1000 m, and 250 m below a depth of 2000 m. The sea ice in each horizontal grid is divided into five categories in addition to open water. The sea ice concentration, ice thickness, and energy of ice melting are predicted for the five categories in a grid cell (Komuro et al., 2012). The lower bounds of ice thickness for these categories are 0.3, 0.6, 1.0, 2.5, and 5.0 m. In the sea ice model, thermodynamic variables for each category, such as sea ice concentration and thickness, are advected by the sea ice horizontal velocity, which conserves ice volume and is common for all categories in a grid.

Historical simulations are performed from 1850 to 2005 using anthropogenic forcings recommended by the CMIP5 project. Historical changes in the solar constant are considered according to Lean et al. (2005). Historical changes in the optical thickness of volcanic stratospheric aerosols are given by Sato et al. (1993), and subsequent updates are available

Atmos. Chem. Phys. Discuss., doi:10.5194/acp-2016-464, 2016
Manuscript under review for journal Atmos. Chem. Phys.
Published: 24 June 2016

Atmospheric Chemistry and Physics
Discussions

(http://data.giss.nasa.gov.modelforce/strataer/). Beginning in 1998, the optical thickness of the volcanic stratospheric aerosols are assumed to exponentially decrease with a one-year relaxation time.

The historical simulation using MIROC5 has five ensemble members with different initial conditions. In this study, monthly mean data are used, and sea ice concentration data are interpolated to correspond with the atmospheric horizontal grids.

3. Results

3.1. Simulated change of Arctic sea ice and clouds

Figure 1a shows the time series of SAT anomalies (ΔSAT) from the 1951-1980 average, which were averaged for both global and the high-latitude regions (60-90°N) during the period 1900-2005. A small increasing trend in the global mean ΔSAT occurred during the period 1900-1960, although the interannual variations of the global mean ΔSAT were dominant. Since the 1970s, the global mean ΔSAT has increased. The increasing trend in the global mean ΔSAT was approximately 0.2 K/decade. Conversely, the ΔSAT (60-90°N) varied between -1.0°C and +1.0°C until 1970. The ΔSAT (60-90°N) began to increase in the 1970s, reaching 1°C in the 2000s. The warming rate from 1976 to 2005 was approximately 0.6 K/decade, which is at least twice as high as the warming rate for the global mean ΔSAT. This result clearly reveals the AA, indicating that the MIROC5 is able to simulate the AA in historical simulations. The positive trend for ΔSAT (60-90°N) for the period 1970-2005 in MIROC5 agrees with the observationally based ΔSAT (60-90°N) data from the Merged Land and Ocean Temperature Analysis (MLOST) (Smith et al., 2008), HadCRUT4 (Morice et al., 2012) and GISS Surface Temperature Analysis (GISTEMP) (Hansen et al., 2010).

Figure 1b shows the time series of the September Arctic sea ice area (SIA). As the SAT in the northern high latitude increased, the Arctic SIA significantly decreased. This decrease from the 1970s was common in all ensemble members. This simulated negative trend in the Arctic SIA averaged for ensemble members agrees with that from the Hadley Center Sea Ice and Sea Surface Temperature data set (HadISST) (Rayner et al., 2003) (Figure 1b), although the simulated SIA is slightly larger than that from the HadISST.

Figure 2a shows the simulated seasonal cycle of the Arctic SIA averaged for the periods 1976-1985 (blue line) and 1991-2005 (red line), and Figure 2b displays the differences in the simulated seasonal cycle. The maximum SIA occurred in March, decreasing to a minimum in August. This seasonal SIA cycle in MIROC5 differs slightly from the observed seasonal cycle (Komuro et al., 2012). According to observations, the seasonal minimum SIA occurs in September, and Arctic sea ice cover generally begins to recover in October. Although discrepancies were found between the observations and our model results, the basic features of the seasonal cycle of the Arctic SIA, such as the summer reduction and fall recovery in SIA, were simulated using MIROC5. Due to recent global warming, the simulated Arctic SIA decreased in all months from 1976 to 2005, displaying a maximum reduction in September. The simulated maximum reduction in the Arctic SIA in September is consistent with observations of the Arctic SIA (Comiso et al., 2008).

Figures 2c and 2d are identical to Figures 2a and 2b except for the total and low-level cloud cover over the Arctic Ocean, respectively. Up to 50% of the Arctic Ocean was covered by low-level clouds in summer. From summer to fall, the simulated cloud cover over the Arctic Ocean decreased, reaching a minimum in April. The simulated seasonal cycle of the total cloud cover was similar to that of low-level clouds. Therefore, in MIROC5, the seasonal cycle of the total cloud cover can be explained by the presence of low-level clouds. Compared with the seasonal cycle of cloud cover observed by the TOVS satellite and surface-based cloud climatology reported by Schweiger et al. (1999) and Hahn et al. (1995), the seasonal cycle of the total cloud cover averaged over the Arctic Ocean was realistically simulated using MIROC5. As shown in Figure 2d, the simulated Arctic cloud cover for fall, winter, and spring increased between 1976-1985 and 1996-2005, although the change was not substantially. The increase in simulated total cloud cover was largest in October, which can also be explained by the increase in low-level cloud coverage. This result agrees with previous studies using satellite data and climate model simulations (Vavrus et al., 2011;Liu et al., 2012;Wu and Lee, 2012). Compared with the low-level cloud cover, the middle- and high-level cloud covers were small in the MIROC5, and their changes between 1976-1985 and 1996-2005 were approximately zero (not shown).

3.2. Relationship between changes in sea ice and cloud cover during the fall

Figure 3 shows the geographical distributions of the simulated linear trends in total cloud cover and sea ice concentrations (SICs) from 1976 to 2005 in September, October, and November. These linear trends were obtained using the least squares method, and the linear trend at each grid was tested for statistical significance to determine whether the trend was zero using a t-test. As shown in Figures 3a and 3b, negative trends in SIC were found over the Laptev Sea, the East Siberian Sea and the Beaufort Sea in September. Additionally, in the Atlantic sector, negative trends were found in the Kara Sea and the Barents Sea. For the cloud cover, a substantial trend was rarely observed and limited to only the coast of the East Siberian Sea and the northern Bering Strait.

Negative trends in SICs remained in October (Figure 3b), although the area of substantial negative trends became narrower than that in September. However, positive trends in cloud cover existed broadly over the Arctic Ocean. In the region of the East Siberian and Beaufort Sea, where SICs markedly decreased, larger positive trends in cloud cover were found.

Atmos. Chem. Phys. Discuss., doi:10.5194/acp-2016-464, 2016
Manuscript under review for journal Atmos. Chem. Phys.
Published: 24 June 2016

Furthermore, the heights of the simulated cloud tops and bases increased predominantly in regions with large reductions in SIC during October, which was also common in September (not shown). This finding implies that increased cloud cover was related to the reduction in SICs in MIROC5. The simulated cloud cover increased substantially over the Arctic Ocean north of the Beaufort Sea, where large negative trends in the simulated SIC were not found. However, in the Barents Sea and near Greenland, significant positive trends in the simulated cloud cover were not found despite the large SIC reduction. Dynamic impacts on the atmosphere from the lower latitude region were strong in the Barents Sea and near Greenland because major atmospheric flows from the lower latitude were found during fall in MIROC5. Thus, the dynamic impact may weaken the thermodynamic effect resulting from the increased open ocean in some ensemble members.

Figure 3c shows that the large negative trends in SIC were limited to the Barents Sea, the Bering Strait and the coasts of Greenland in November. Over these regions, a significant increase in cloud cover was found. This result also supports the model results in which cloud cover increases because of reduced sea ice. In winter months, cloud cover increased over grids with reduced sea ice, similar to that in November (not shown). However, the simulated cloud cover change averaged over the Arctic Ocean in November and winter months was less dominant than that in October because the sea ice reductions were smaller. The following paragraphs focus on the increased cloud cover in October.

Figures 4a and 4b show the geographical distribution of one-month-lagged autocorrelations of simulated sea ice concentrations between September and October and instantaneous correlations of simulated cloud cover and sea ice concentrations in October, respectively. The correlation coefficients were calculated for the period 1976-2005. For the autocorrelation in sea ice concentration between September and October, large positive correlation coefficients were found over most of the Arctic Ocean, with larger values exceeding 0.6 over the lower latitude

Atmos. Chem. Phys. Discuss., doi:10.5194/acp-2016-464, 2016
Manuscript under review for journal Atmos. Chem. Phys.
Published: 24 June 2016

regions from the Beaufort Sea to the Barents Sea (Fig. 4a). In the Arctic subregion exhibiting a high autocorrelation of simulated SIC (109-221°E, 69-78°N), which is shown in Fig. 4a with black broken lines, the autocorrelations of the simulated SIC (blue circle in Fig. 4c) decayed with a slower time lag than those of the simulated cloud cover (black circle in Fig. 4c) because the autocorrelations of the simulated SIC reflect a substantially longer memory in sea ice. These results suggest that sea ice changes in October tend to depend on sea ice changes in September in MIROC5; small SIC during September is likely to results in small SIC during October.

Stronger negative correlations between SIC and cloud cover in October were found in grids with large negative trends in SIC during the period 1976-2005 (Fig. 4b). This finding indicates that increased cloud cover in the grids was associated with a smaller SIC. The negative relationship between SIC and cloud cover in MIROC5 agrees with the observed results in Palm et al. (2010) and Liu et al. (2012). Lead/lag correlations in the Arctic subregion demonstrated that cloud cover in October was negatively correlated with the lead/lagged SIC (green diamond in Fig. 4c). This negative correlation of cloud cover in October with SIC in September suggested that small SIC continuing from September led to increased cloud cover in October because a strong autocorrelation of SIC between September and October was found. Additionally, because the autocorrelation of the simulated cloud cover between September and October was weaker than the correlation between the simulated cloud cover in October and simulated SIC in September, the increased cloud cover in October is unlikely to represent a continuing increase in cloud cover from September in MIROC5. However, SIC in October was also negatively correlated with lead/lagged cloud cover (red diamond in Fig. 4c). The correlation of SIC in October and cloud cover in September was weaker than that of cloud cover in October and SIC in September. Therefore, we concluded that cloud cover is likely to increase due to a decrease in SIC during October in MIROC5. This result supports previous findings with satellite data in Liu et al. (2012) in which decreases in SIC lead to increases in cloud cover.

Atmos. Chem. Phys. Discuss., doi:10.5194/acp-2016-464, 2016
Manuscript under review for journal Atmos. Chem. Phys.
Published: 24 June 2016

Atmospheric Chemistry and Physics Discussions

Although the correlation of cloud cover in October and SIC in November was strong in the MIROC5 simulations (red diamond in Fig. 4c), the autocorrelation of sea ice between October and November remained strong. Thus, changes in SIC in November may be strongly reflected by those in October rather than the impact of cloud cover in October on SIC in November. Importantly, because this correlation analysis used monthly mean data, correlations between variables at time scales smaller than one month remain unclear.

We also conducted systematic sensitivity experiments using MIROC5-AGCM to examine the effect of reduced sea ice on Arctic cloud cover. The experiments showed that a large reduction in sea ice caused an increase in cloud cover in fall (the details are described in the Appendix). We also confirmed that increased Arctic cloud cover depends strongly on reductions in sea ice; for example, when sea ice is substantially reduced, even if the SST in the 1980s remains constant, Arctic cloud cover increases in MIROC5-AGCM. These findings support the above results from the historical MIROC5 simulations.

3.3. Cloud cover changes resulting from reduced sea ice

As shown in Figure 3, the retreating Arctic sea ice in September and October was substantial in the MIROC5 simulations, although the positive trends in cloud cover in September were less than those in October. As the open ocean extends because of reduced sea ice, vertical heat and moisture fluxes from the ocean to the atmosphere are enhanced. Figure 5 shows simulated linear trends in the latent heat (LE) and sensible heat (SH) fluxes in September and October. Positive trends were identified in the LE and SH fluxes in grids with substantially reduced sea ice coverage. The increase in both fluxes was larger in October than in September because of the large temperature difference between the atmosphere and the sea surface in October. Because the air temperature typically decreases from September to October, the difference between the air temperature and sea surface temperature was greater in October compared with that in September, causing the two fluxes to increase. The increased LE and SH fluxes may play a role in the increased cloud cover in October. These results are also consistent with previous studies (Schweiger et al., 2008;Vavrus et al., 2011;Blüthgen et al., 2012).

Figure 6 shows comparisons of the simulated vertical profiles of the cloud fraction, relative humidity, specific humidity, and air temperature in October between grids with and without large reductions in sea ice. In this figure, the "Δai-" case is defined by grids with a linear trend in SIC of less than -0.1/decade. As shown in Fig. 3b, many of the Δai- grids were located over a broad region, including the Laptev Sea, the East Siberian Sea and the Beaufort Sea. The "Δai+" case is defined by grids with linear trends in SIC exceeding -0.1/decade over a restricted latitude band (i.e., 65°-73°N). This limited latitude band was included because the Δai- grids are located mainly in this latitude band. In the Δai- case, an increase in the cloud fraction was found in the lower troposphere centered at the σ=0.9 level (approximately 830 m) (Figures 6a and 6b). At the σ=0.9 level, the cloud fraction increased by approximately 15%. For the increased cloud fraction, the cloud liquid water increased through large-scale condensation, although the cloud ice showed little change. However, the cloud fraction decreased at levels below σ=0.95. The cloud base height rose because of the reduced sea ice in the Δai- case (not shown). Figures 6c and 6d show that the relative humidity increased at levels between σ=0.9 and σ=0.8 (approximately 1839 m) for the Δai- case. This result was found to be consistent with the increased cloud fraction. Decreased relative humidity was also found at levels below σ=0.9, consistent with the decreased cloud fraction at levels below σ=0.95 (approximately 460 m). Features of the simulated vertical structures of cloud fraction and relative humidity in the latter period for the Δai- are very similar to those for low sea ice years in the ERA-interim data set in Cuzzone and Vavrus (2011) and those for below-normal ice concentration in ERA-40 data set in Schweiger et al. (2008), although the values in this study differ from those in the reanalysis data sets. In the reanalysis data sets, the cloud fraction and relative humidity in the layers near the surface are smaller than those in the overlying layers. Furthermore, our results are consistent with those of the satellite measurements of Palm et al. (2010), which showed increased autumnal clouds within 500 m of the surface over sea ice rather than open ocean.

Figures 6e and 6f show that the specific humidity in the lower troposphere increased more dramatically in the Δai- case than in the Δai+ case, although increases in the specific humidity at all levels were found for both cases (Fig. 6f). Compared with the change in the saturated specific humidity (*qsat*, dot-dot-dash lines in Figures 6e and 6f), the increase in the specific humidity in the Δai- case was similar to that for *qsat* at levels with increased cloud fraction. Therefore, the relative humidity increased and enhanced the cloudiness at these levels (Figures 6b and 6d). However, the increases in the specific humidity were smaller than those in *qsat* at thin layers near the surface. The large increase in *qsat* within these thin layers was attributable to large increases in air temperature in the Δai- case. Figures 6g and 6h show that the air temperature increased; the maximum increase occurred at the surface. Substantial increases in air temperature in the Δai- case were found between the surface and σ=0.85 (approximately 1200 m) (Figure 6f). Therefore, in the thin surface layers, the relative humidity decreased, which reduced cloudiness. These changes in the simulated vertical structures of air temperature and specific humidity between the earlier and latter periods for the Δai- case correspond with differences in those between low sea ice years and high sea ice years in the ERA-interim dataset in Cuzzone and Vavrus (2011), although the differences in cloud fractions in the layers near the surface are much larger in the ERA-interim data set.

The lapse rate of the specific humidity in the Δai- case became large throughout most of the lower tropospheric levels in the latter period compared with the Δai+ case (Fig. 6e). This increase in the lapse rate of the specific humidity in MIROC5 reflected an increase in water vapor from the open ocean and an enhancement in the vertical water cycle, including convection, cloud, and precipitation processes because simulated cloud fractions and precipitation increase in addition to evaporation from the open ocean. Much more water vapor from the open ocean can be vertically transported to higher levels by vertical mixing and convection, and the transported water vapor can then be removed from the atmosphere through phase changes in cloud and precipitation processes at the levels in which cloud fractions increased. As a result, the lapse rate of the specific humidity may not decrease in the lower tropospheric. Thus, these processes can effectively transport water vapor from the surface of the open ocean to higher levels, contributing to increased cloud cover and precipitation. However, in the Δai+ case, vertical diffusion (turbulent mixing) of water vapor was weak; the lapse rate of the specific humidity was small in the layers near the surface. However, in this interpretation of the enhanced vertical water cycle, the effects of the horizontal advection of water vapor were not considered because the horizontal effect was obscured by averaging the data for grids and ensemble members in the composite analysis.

The lapse rate of the simulated air temperature was extremely large in the thin layers close to the surface in the Δai- case (Fig. 6g). Increased sensible heat and longwave radiation from the ocean to the atmosphere resulted in large increases in air temperature because the SSTs in the open ocean were near zero and much higher than the air temperature. Furthermore, radiative cooling in all atmospheric levels contribute to the smaller lapse rates in the air temperature at all layers except the thin surface layer. Thus, strong heat diffusion (turbulent mixing) was confined to the thin surface layers in the MIROC5 simulations.

In the Δai+ case, the humidity and air temperature increased in the lower troposphere likely because of global warming. Thus, the effect of global warming on the atmosphere, particularly in the boundary layer, appeared in a region of the Arctic Ocean without a reduction in sea ice; however, the effect was small.

Atmos. Chem. Phys. Discuss., doi:10.5194/acp-2016-464, 2016
Manuscript under review for journal Atmos. Chem. Phys.
Published: 24 June 2016

Atmospheric Chemistry and Physics Discussions

3.4. Cloud radiative forcing

Cloud cover changes can affect the energy balance through the cloud radiative forcing (CRF). During the fall, winter, and spring seasons in the Arctic region, the DLR by clouds may play an important role in the surface energy balance because of the reduced or absent incoming shortwave radiation. In addition, increasing the DLR because of increased water vapor content and air temperature is an important factor contributing to Arctic warming (Rinke et al., 2013).

Figure 7a shows the change in CRF for both the surface DLR (ΔCRF_{SDLR}) and clear-sky surface DLR (ΔCS_{SDLR}) between the periods, 1976-1985, and 1996-2005. The changes denoted in the figure were averaged for the Δai- grids and Δai+ grids in each month. Positive ΔCS_{SDLR} was found in both cases. Positive ΔCS_{SDLR} was dominant in the Δai- case when compared with the Δai+ case, particularly during fall, winter, and spring. This positive ΔCS_{SDLR} resulted from both warming and moistening due to the increased open ocean and global warming. Thus, positive ΔCS_{SDLR} due to increased water vapor and air temperature can largely affect the surface energy balance in the grids with dramatically reduced SIC.

Positive large ΔCRF_{SDLR} in the Δai- case was found during the period September-April; the changes in the Δai+ case was small. This result suggested that increased CRF of surface DLR was not negligible and potentially contributed to the increased radiation energy into the surface in the grids with substantially reduced SIC. However, compared with the large positive ΔCS_{SDLR}, ΔCRF_{SDLR} was smaller.

During the summer, large positive ΔCS_{SDLR} and small ΔCRF_{SDLR} were found in both cases, although the differences between the cases were very small. This result indicated that reduced sea ice was unlikely to enhance differences in the variation of surface DLR during summer in the MIROC5 simulations.

Atmos. Chem. Phys. Discuss., doi:10.5194/acp-2016-464, 2016
Manuscript under review for journal Atmos. Chem. Phys.
Published: 24 June 2016

Atmospheric Chemistry and Physics Discussions

To further analyze the model simulations, we introduce an index defined by the ratio between ΔCRF_{SDLR} and ΔCS_{SDLR} ($(\Delta CRF/\Delta CS)_{SDLR}$). Using this index, we evaluated the relative importance of changes in CRF of surface DLR to the large changes in clear-sky surface DLR. Figure 7b shows the annual time series of $(\Delta CRF/\Delta CS)_{SDLR}$. The figure shows that ΔCRF_{SDLR} was positive in grids in which the sea ice was reduced because the cloud cover increased from reduced sea ice during fall, winter, and spring, although this was negative during summer (Fig. 7a). Additionally, ΔCS_{SDLR} was positive over the entire Arctic Ocean because of increased air temperature and moisture (Fig. 7a). The indexes in Figure 7b were approximately 0.4-0.7 during fall, winter and early spring, varying between the seasons. Although the indexes during winter were larger than those in fall, the uncertainties (error bars) were large during winter. Furthermore, the uncertainties in the indexes during spring were also large. The greater uncertainties were due to the small sample numbers of Δai- grids during both winter and spring. Thus, it was difficult to obtain a statistically significant result for the indexes during winter and spring. Furthermore, as described above, no substantial differences were found between the clear-sky surface DLR and the CRF of the surface DLR during summer. This result was common in the indexes during summer, showing no substantial differences in the indexes between the Δai- and Δai+ cases (Fig. 7b).

By contrast, uncertainties in the indexes from October to December were small in both the Δai- and Δai+ cases. An increase in the cloud cover as a result of reduced sea ice enhanced the surface DLR. The indexes during the period October-December showed that the all-sky surface DLR in the Δai- cases increased by approximately 40-60% compared with the clear-sky surface DLR. The indexes in the Δai- grids were larger than those in the Δai+ grids, although the index in the Δai- grids in November was not clearly distinguished from that in the Δai+ grids. Thus, considering the reduction of sea ice in October, the change in the CRF due to reduced sea ice was not disregarded as a factor affecting Arctic warming. This finding disagrees with Rinke et

Atmos. Chem. Phys. Discuss., doi:10.5194/acp-2016-464, 2016
Manuscript under review for journal Atmos. Chem. Phys.
Published: 24 June 2016

Atmospheric Chemistry and Physics
Discussions

al. (2013). However, the index shown in Figure 7b differed from the averaged value over the Arctic Ocean. The averaged value was smaller in winter and early spring because the area with significant sea ice reduction was small during these seasons.

We also compared the change in CRF of the surface downward shortwave radiation (DSR) with clear-sky surface DSR in both the Δai- and Δai+ cases The change in the CRF of the surface DSR in the Δai+ case was a small fraction of the clear-sky surface DSR over the year. The result in the Δai- case showed that the change in the CRF of the surface DSR was less than 10 percent of clear-sky surface DSR during summer, fall and winter, and the change during spring had a large uncertainty in the Δai- case (not shown). In addition, clear-sky surface DSR was close to zero during winter. Therefore, we concluded that the impact of cloud cover changes resulting from reduced sea ice on the surface DSR was small during the fall.

4. Discussion

As shown in Figure 3b, increases in the simulated cloud cover were found in the Arctic Ocean near the North Pole, where simulated sea ice did not decrease substantially. We investigated the effect of changes in both the moisture convergence and the static stability in the lower troposphere on the simulated increased cloud cover. Figure 8a shows the simulated linear trend in the sea level pressure (SLP), moisture flux at 925 hPa, and the convergence in October, which were averages of the ensemble members. The figure shows that the moisture flux converged in the region with increased cloud cover. Therefore, the cloud cover in the region near the North Pole increased in the lower troposphere due to moisture convergence despite the absence of a significant reduction in sea ice. However, by analyzing the data in each ensemble member, we found several ensemble members in which increases in moisture convergence in regions without large reductions in sea ice did not lead to increased cloud cover. Therefore, enhanced

Atmos. Chem. Phys. Discuss., doi:10.5194/acp-2016-464, 2016
Manuscript under review for journal Atmos. Chem. Phys.
Published: 24 June 2016

Atmospheric Chemistry and Physics
Discussions
Open Access

moisture convergence may be insufficient to result in increased cloud cover. Furthermore, Figure 8b shows the simulated linear trend in the lapse rate of equivalent potential temperature between the surface and σ=0.9, which was also averaged for the ensemble members. The figure shows that the static stability in the lower troposphere decreased over the Arctic Ocean, although large decreases in static stability did not always correspond with large increases in cloud cover in regions without large reductions in sea ice. This result was common in each ensemble member. Therefore, an appropriate and systematic cause of the large increases in cloud cover over the region without substantial reduction in sea ice remains unclear. To clarify this finding, more ensemble members may be required in the experiment.

Under global warming conditions, both air temperature and humidity increase, complicating the changes in Arctic cloud cover. Therefore, considering future Arctic cloud cover changes, increases in both air temperature and humidity are crucial components in addition to sea ice loss. With regard to the vertical profile of cloud cover changes, the level at which air temperature and humidity increase under global warming conditions is important. Thus, fine vertical resolution and boundary processes in the model may be primary factors for improving the projections of Arctic cloud cover change related to global warming and sea ice loss in the future.

Previous studies have argued for the role of changes in Arctic cloud cover in Arctic warming. Significantly increased DLR due to cloud cover occurred in grids with significant reductions in sea ice, whereas select studies have noted a reduced effect caused by the increase in cloud cover on the surface DLR. These discrepancies should be related to the uncertainties of clouds and cloud radiative forcing in individual models. The vertical profile of changes in cloud cover is also strongly related to changes in cloud radiative forcing. Uncertainty in air temperature and humidity increases may be among the causes. Therefore, further investigations into Arctic cloud cover changes and feedback processes related to clouds are needed.

Atmos. Chem. Phys. Discuss., doi:10.5194/acp-2016-464, 2016
Manuscript under review for journal Atmos. Chem. Phys.
Published: 24 June 2016

Atmospheric Chemistry and Physics Discussions

With regard to the feedback between sea ice and clouds, the effects of cloud cover on sea ice are also considerable. This study focused on the changes in Arctic cloud cover as a result of reduced sea ice. However, we were unable to observe an effect of increased cloud cover on sea ice reduction in our statistical analysis of inter-seasonal variations using monthly mean data despite the increased surface DLR resulting from increased cloud cover.

5. Summary

This study investigated Arctic cloud cover changes resulting from reduced sea ice due to global warming simulated by MIROC5 to understand the effect of changes in the extent of Arctic sea ice on cloud cover.

A large negative trend was found for Arctic sea ice in the MIROC5 simulations in summer and fall during the period 1976-2005, although small negative trends in the winter and spring were found in limited regions. The temporal trend in the simulated Arctic cloud cover was positive in fall, winter, and spring, reaching a maximum in October. This study focused on increases in the cloud fraction in October resulting from reduced sea ice.

In grids with reduced SICs (trends of less than -0.1 /decade) in the MIROC5 simulations, the cloud fraction in October increased at levels between σ=0.9 and σ=0.7. Because of the reduced sea ice, a more extensive open ocean area increased the latent and sensible heat fluxes from the ocean to the atmosphere. Along with the seasonal progression, decreased atmospheric temperatures increased the temperature gradient between the air and sea surface in October. Therefore, the fluxes from the ocean to the atmosphere were enhanced in October rather than in September. This effect resulted in a greater increase in the cloud fraction in October than in September. However, because extreme warming was found in the thin surface layer, the cloud fraction decreased in this layer in the MIROC5 simulations. In addition, from the large lapse rate of specific humidity throughout the lower troposphere in grids with reduced SIC and increased clouds and precipitation, we concluded that vertical water cycles, including both cloud and precipitation processes, were enhanced by the reduction in sea ice based on the MIROC5 simulations. Thus, water vapor was effectively transported to higher levels, at which point cloud fractions increased due to vertical mixing.

There were several ensemble members in which the cloud cover increased in regions close to the North Pole, where no substantial reductions in sea ice were simulated. However, a plausible cause for this increase in the simulated cloud cover remains unclear despite our analysis on the changes in water vapor convergence and the static stability in the lower troposphere in each ensemble member. To clarify this dichotomy, more ensemble members may be required in the experiment.

The change in CRF as a result of reduced sea ice in the surface DLR was approximately 40-60% compared with a change in clear-sky surface DLR, which was considered as a change in the surface DLR due to increases in air temperature and water vapor in grids with large sea ice reductions in fall. Therefore, the change in CRF resulting from reduced sea ice must be considered as a factor influencing Arctic warming.

This study analyzed data from only one climate model, i.e., MIROC5. Therefore, future research topics include the sea ice–cloud cover relationship in multiple models and its contribution to the uncertainty of future climate change projections. In the future, if the sea ice retreats further in summer, fall, and spring, then the Arctic cloud cover could increase further, and the effects of cloud cover could become stronger. Thus, further understanding and correct projections of the relationship between sea ice and cloud cover are important for the analysis of future global and Arctic climate change.

Atmos. Chem. Phys. Discuss., doi:10.5194/acp-2016-464, 2016
Manuscript under review for journal Atmos. Chem. Phys.
Published: 24 June 2016

Atmospheric Chemistry and Physics Discussions
Open Access

Appendix

A. Sensitivity of Arctic cloud cover to sea ice reductions

A1. Sensitivity experiments with MIROC5-AGCM

To further examine the effect of reduced sea ice on Arctic cloud cover, we conducted systematic sensitivity experiments with MIROC5-AGCM. In the sensitivity experiments, the Arctic cloud cover under different SST and sea ice conditions in the 1980s and 2000s were compared. Additionally, the impact of changes in other forcings, such as greenhouse gases, aerosols, and land use, from the 1980s to 2000s on the Arctic cloud cover were examined. Table A1 shows the SST, sea ice, and other forcing conditions. These experiments used climatological monthly mean SST and sea ice data, which were obtained from historical MIROC5 simulations. The SST and SIC in the 1980s were averages over the period 1976-1985 in the historical simulations. Moreover, both the SST and SIC in the 2000s comprised additive data from the 1980s and changes for the following 20 years, which were estimated using the linear trend from 1976 to 2005 in the historical simulations. Because we had five ensemble members in the historical simulations, each of the sensitivity experiments consisted of five ensemble members, in which combinations of the SST and sea ice based on each member of the historical simulations were prescribed. Other conditions, such as greenhouse gases, aerosols, and total solar irradiance, in the CTL and other simulations corresponded to those in 1980 and 2000. The sensitivity experiments were integrated for 30 years, and the last 20 years were used in this analysis.

A2. Results

Figure A1a shows the annual cycle of cloud cover averaged for the Arctic Ocean. The annual cycle for the all simulations was similar to that of the historical MIROC5 simulations, although

Atmos. Chem. Phys. Discuss., doi:10.5194/acp-2016-464, 2016
Manuscript under review for journal Atmos. Chem. Phys.
Published: 24 June 2016

Atmospheric Chemistry and Physics
Discussions

the cloud coverage in July and August (from October to May) was slightly smaller (larger) than that in the historical simulations.

Figure A1b shows the annual cycle of cloud cover differences from the CTL simulation in each experiment. During fall, the cloud cover differences in the IA2K and TIA2K experiments were largest, which was similar to the historical simulations shown in Fig. 2d. Because the cloud cover increased primarily in grids without large decreases in sea ice in November, we focused on the differences in cloud cover in October because increased cloud cover in October was the focus of the historical simulation analysis.

Figure A2 shows the geographical maps of cloud cover in October for the CTL and ITA2K experiments and differences in cloud cover in the experiments from the CTL simulation. Increased cloud cover due to sea ice reductions was found in the IA2K and ITA2K experiments (Figs. A2d and A2f). In the IA2K and ITA2K experiments, increased cloud cover appeared in grids with large sea ice reductions, although similar changes were in cloud cover were also found for small reductions in sea ice. Conversely, large increases in cloud cover were not found in the A2K and TA2K experiments (Figs. A2c and A2e). These results suggested that large sea ice reductions caused the increased cloud cover. Additionally, as shown in Figure A2d, even if the SST in the 1980s remained constant, cloud cover increased in October when sea ice was reduced. Furthermore, changes in the SST and other conditions (except sea ice) from the 1980s to 2000s did not increase cloud cover, as shown in Figs. A2c and A2e. Therefore, increased Arctic cloud cover in the MIROC5-AGCM simulations was found to depend strongly on sea ice reductions. These results support the results from the historical MIROC5 simulations in which increased Arctic clouds were caused by large sea ice reductions.

Unfortunately, using these sensitivity experiments, we could not assess the impact of increased cloud cover on sea ice reduction, which is a future consideration.

Atmos. Chem. Phys. Discuss., doi:10.5194/acp-2016-464, 2016
Manuscript under review for journal Atmos. Chem. Phys.
Published: 24 June 2016

Atmospheric Chemistry and Physics
Discussions
Open Access
EGU

Acknowledgments

We thank Y. Komuro and T. Suzuki for providing the land fraction data for MIROC5 to enable the calculations of the Arctic sea ice area. Additionally, we thank two anonymous referees for the valuable comments to improve the manuscript. This study was supported by the GRENE Arctic Climate Change Research Project and the Arctic Challenge for Sustainability (ArCS) Project conducted by the Ministry of Education, Culture, Sports, Science and Technology of the Japanese Government. The Earth Simulator at JAMSTEC was employed to perform the AOGCM simulations.

References

Blüthgen, J., Gerdes, R., and Werner, M.: Atmospheric response to the extreme Arctic sea ice conditions in 2007, Geophys. Res. Lett., 39, L02707, 10.1029/2011gl050486, 2012.

Comiso, J. C.: Warming Trends in the Arctic from Clear Sky Satellite Observations, Journal of Climate, 16, 3498-3510, 10.1175/1520-0442(2003)016<3498:WTITAF>2.0.CO;2, 2003.

Comiso, J. C., Parkinson, C. L., Gersten, R., and Stock, L.: Accelerated decline in the Arctic sea ice cover, Geophys. Res. Lett., 35, L01703, 10.1029/2007GL031972, 2008.

Curry, J. A., Schramm, J. L., and Ebert, E. E.: Sea Ice-Albedo Climate Feedback Mechanism, Journal of Climate, 8, 240-247, 10.1175/1520-0442(1995)008<0240:SIACFM>2.0.CO;2, 1995.

Cuzzone, J., and Vavrus, S.: The relationships between Arctic sea ice and cloud-related variables in the ERA-Interim reanalysis and CCSM3, Environmental Research Letters, 6, 014016, 2011.

Dickinson, R., Meehl, G., and Washington, W.: Ice-albedo feedback in a CO2-doubling simulation, Climatic Change, 10, 241-248, 10.1007/BF00143904, 1987.

Hahn, C. J., Warren, S. G., and London, J.: The Effect of Moonlight on Observation of Cloud Cover at Night, and Application to Cloud Climatology, Journal of Climate, 8, 1429-1446, 10.1175/1520-0442(1995)008<1429:TEOMOO>2.0.CO;2, 1995.

Hansen, J., Ruedy, R., Sato, M., and Lo, K.: GLOBAL SURFACE TEMPERATURE CHANGE, Reviews of Geophysics, 48, RG4004, 10.1029/2010RG000345, 2010.

Hasumi, H.: CCSR Ocean Component Model (COCO), version 4.0, 103, 2007.

Holland, M. M., and Bitz, C. M.: Polar amplification of climate change in coupled models, Climate Dynamics, 21, 221-232, 10.1007/s00382-003-0332-6, 2003.

Kay, J. E., and Gettelman, A.: Cloud influence on and response to seasonal Arctic sea ice loss, Journal of Geophysical Research: Atmospheres, 114, D18204, 10.1029/2009JD011773, 2009.

Komuro, Y., Suzuki, T., Sakamoto, T. T., Hasumi, H., Ishii, M., Watanabe, M., Nozawa, T., Yokohata, T., Nishimura, T., Ogochi, K., Emori, S., and Kimoto, M.: Sea-Ice in Twentieth-Century Simulations by New MIROC Coupled Models: A Comparison between Models with High Resolution and with Ice Thickness Distribution, Journal of Meteorological Society of Japan, 90A, 213-232, 2012.

Lean, J., Rottman, G., Harder, J., and Kopp, G.: SORCE Contributions to New Understanding of Global Change and Solar Variability, Sol Phys, 230, 27-53, 10.1007/s11207-005-1527-2, 2005.

Liu, Y., Key, J. R., Liu, Z., Wang, X., and Vavrus, S. J.: A cloudier Arctic expected with diminishing sea ice, Geophys. Res. Lett., 39, n/a-n/a, 10.1029/2012gl051251, 2012.

Manabe, S., and Stouffer, R. J.: Sensitivity of a global climate model to an increase of CO2 concentration in the atmosphere, Journal of Geophysical Research: Oceans, 85, 5529-5554, 10.1029/JC085iC10p05529, 1980.

Morice, C. P., Kennedy, J. J., Rayner, N. A., and Jones, P. D.: Quantifying uncertainties in global and regional temperature change using an ensemble of observational estimates: The HadCRUT4 data set, Journal of Geophysical Research: Atmospheres, 117, D08101, 10.1029/2011JD017187, 2012.

Palm, S. P., Strey, S. T., Spinhirne, J., and Markus, T.: Influence of Arctic sea ice extent on polar cloud fraction and vertical structure and implications for regional climate, Journal of Geophysical Research: Atmospheres, 115, n/a-n/a, 10.1029/2010JD013900, 2010.

Perovich, D. K., Light, B., Eicken, H., Jones, K. F., Runciman, K., and Nghiem, S. V.: Increasing solar heating of the Arctic Ocean and adjacent seas, 1979–2005: Attribution and role in the ice-albedo feedback, Geophys. Res. Lett., 34, L19505, 10.1029/2007GL031480, 2007.

Porter, D. F., Cassano, J. J., and Serreze, M. C.: Local and large-scale atmospheric responses to reduced Arctic sea ice and ocean warming in the WRF model, Journal of Geophysical Research: Atmospheres, 117, D11115, 10.1029/2011JD016969, 2012.

Rayner, N. A., Parker, D. E., Horton, E. B., Folland, C. K., Alexander, L. V., Rowell, D. P., Kent, E. C., and Kaplan, A.: Global analyses of sea surface temperature, sea ice, and night marine air temperature since the late nineteenth century, Journal of Geophysical Research: Atmospheres, 108, 4407, 10.1029/2002JD002670, 2003.

Rinke, A., Dethloff, K., Dorn, W., Handorf, D., and Moore, J. C.: Simulated Arctic atmospheric feedbacks associated with late summer sea ice anomalies, Journal of Geophysical Research-Atmospheres, 118, 7698-7714, Doi 10.1002/Jgrd.50584, 2013.

Sato, K., Inoue, J., Kodama, Y.-M., and Overland, J. E.: Impact of Arctic sea-ice retreat on the recent change in cloud-base height during autumn, Geophys. Res. Lett., 39, n/a-n/a, 10.1029/2012gl051850, 2012.

Sato, M., Hansen, J. E., McCormick, M. P., and Pollack, J. B.: Stratospheric aerosol optical depths, 1850–1990, Journal of Geophysical Research: Atmospheres, 98, 22987-22994, 10.1029/93JD02553, 1993.

Schweiger, A. J., Lindsay, R. W., Key, J. R., and Francis, J. A.: Arctic clouds in multiyear satellite data sets, Geophys. Res. Lett., 26, 1845-1848, 10.1029/1999GL900479, 1999.

Schweiger, A. J.: Changes in seasonal cloud cover over the Arctic seas from satellite and surface observations, Geophys. Res. Lett., 31, L12207, 10.1029/2004GL020067, 2004.

Schweiger, A. J., Lindsay, R. W., Vavrus, S., and Francis, J. A.: Relationships between Arctic Sea Ice and Clouds during Autumn, Journal of Climate, 21, 4799-4810, 10.1175/2008JCLI2156.1, 2008.

Screen, J. A., and Simmonds, I.: Increasing fall-winter energy loss from the Arctic Ocean and its role in Arctic temperature amplification, Geophys. Res. Lett., 37, L16707, 10.1029/2010GL044136, 2010.

Serreze, M. C., and Barry, R. G.: Processes and impacts of Arctic amplification: A research synthesis, Global and Planetary Change, 77, 85-96, http://dx.doi.org/10.1016/j.gloplacha.2011.03.004, 2011.

Smith, T. M., Reynolds, R. W., Peterson, T. C., and Lawrimore, J.: Improvements to NOAA's Historical Merged Land–Ocean Surface Temperature Analysis (1880–2006), Journal of Climate, 21, 2283-2296, 10.1175/2007JCLI2100.1, 2008.

Vavrus, S., Waliser, D., Schweiger, A., and Francis, J.: Simulations of 20th and 21st century Arctic cloud amount in the global climate models assessed in the IPCC AR4, Climate Dynamics, 33, 1099-1115, 10.1007/s00382-008-0475-6, 2009.

Vavrus, S., Holland, M. M., and Bailey, D. A.: Changes in Arctic clouds during intervals of rapid sea ice loss, Climate Dynamics, 36, 1475-1489, DOI 10.1007/s00382-010-0816-0, 2011.

Wang, X., and Key, J. R.: Recent trends in Arctic surface, cloud, and radiation properties from space, Science, 299, 1725-1728, 10.1126/science.1078065, 2003.

Watanabe, M., Suzuki, T., O'ishi, R., Komuro, Y., Watanabe, S., Emori, S., Takemura, T., Chikira, M., Ogura, T., Sekiguchi, M., Takata, K., Yamazaki, D., Yokohata, T., Nozawa, T., Hasumi, H., Tatebe, H., and Kimoto, M.: Improved Climate Simulation by MIROC5: Mean States, Variability, and Climate Sensitivity, Journal of Climate, 23, 6312-6335, 10.1175/2010jcli3679.1, 2010.

Wu, D. L., and Lee, J. N.: Arctic low cloud changes as observed by MISR and CALIOP: Implication for the enhanced autumnal warming and sea ice loss, Journal of Geophysical Research: Atmospheres, 117, D07107, 10.1029/2011JD017050, 2012.

Yoshimori, M., Abe-Ouchi, A., Watanabe, M., Oka, A., and Ogura, T.: Robust Seasonality of Arctic Warming Processes in Two Different Versions of the MIROC GCM, Journal of Climate, 27, 6358-6375, 10.1175/JCLI-D-14-00086.1, 2014.

Atmos. Chem. Phys. Discuss., doi:10.5194/acp-2016-464, 2016
Manuscript under review for journal Atmos. Chem. Phys.
Published: 24 June 2016

Figure Captions

Figure 1. a) Time series of the surface air temperature (SAT) anomaly from the 1951-1980 mean. Solid black, green, orange, and blue lines are the SAT anomalies averaged over 60-90°N in MIROC5's ensemble mean, MLOST, GISTEMP, and HadCRUT4, respectively. The broken black line is the global and ensemble mean SAT anomaly in MIROC5. The gray shaded area indicates the maximum and minimum SAT anomalies between the ensemble members of MIROC5. b) Time series of the September sea ice extent. The black lines represent the ensemble mean. The gray shaded area indicates the maximum and minimum ensemble members. The purple line is the September sea ice extent calculated from HadISST. The units of the SAT anomaly and sea ice extent anomaly are K and 10^6 km^2, respectively.

Figure 2. Seasonal cycle of a) Arctic mean sea ice area averaged over the periods 1976-1985 and 1996-2005 in MIROC5 and b) the difference between the means; c) and d) are identical to a) and b) except for the total and low cloud covers. The unit of sea ice area is 10^6 km^2.

Figure 3. Geographical map of the simulated linear trend in the total cloud cover (shaded) and sea ice concentration (contours) in (a) September, (b) October, and (c) November during the period 1976-2005. The units are decade^{-1}. Dots indicate that the linear trend is not zero at the 95% significance level.

Figure 4. a) Autocorrelation coefficients in the sea ice concentration between September and October in the MIROC5 simulations. b) Correlation coefficients between cloud cover and sea

Atmos. Chem. Phys. Discuss., doi:10.5194/acp-2016-464, 2016
Manuscript under review for journal Atmos. Chem. Phys.
Published: 24 June 2016

ice concentration in October in the MIROC5 simulations. c) Autocorrelation (closed circles) in the sea ice concentration (blue solid lines) and cloud cover (black solid lines), correlations (closed diamonds) in the lead/lagged sea ice concentrations and October cloud cover (green broken lines), and correlations in the October sea ice concentration and lead/lagged cloud cover (red broken lines) in the MIROC5 simulations. The correlation coefficients were calculated using averages for the boxed region shown in a).

Figure 5. Geographical map of the simulated linear trend in (a, b) latent heat and (c, d) sensible heat fluxes in (a, c) September and (b, d) October during the period 1976-2005. The units are W m^{-2} $decade^{-1}$. A linear trend for the sea ice concentration (contours) is overlaid, and the units are $decade^{-1}$.

Figure 6. Vertical profiles of the average a) cloud fraction, c) relative humidity, e) specific humidity, and g) air temperature in October in the MIROC5 simulations for the periods 1976-1985 (blue) and 1996-2005 (red). The solid (broken) line represents the Δai- (Δai+) case. See the text for the definitions of the Δai- and Δai+ cases. Vertical profiles of the differences between average b) cloud fraction, d) relative humidity, f) specific humidity, and h) air temperature in October in the MIROC5 simulations for the periods 1976-1985 and 1991-2005. The solid (broken) line represents the Δai- (Δai+) case. The dot-dot-dash lines in e) and f) indicate the saturated specific humidity. The units of air temperature and specific humidity are K and g kg^{-1}, respectively. Shading and error bars indicate the standard deviations for the ensemble members in the Δai- and Δai+ cases, respectively.

Atmos. Chem. Phys. Discuss., doi:10.5194/acp-2016-464, 2016
Manuscript under review for journal Atmos. Chem. Phys.
Published: 24 June 2016

Atmospheric Chemistry and Physics Discussions
Open Access
EGU

Figure 7. Annual time series of a) the change in (crosses) the CRF in surface DLR (ΔCRF_{SDLR}) and (closed circles) clear-sky surface DLR (ΔCS_{SDLR}) between the averages for 1976-1985 and 1996-2005 in the MIROC5 simulations and b) $(\Delta CRF/\Delta CS)_{SDLR}$. The solid red (broken black) lines indicate the Δai- (Δai+) case. See the text for the definition of the index. Shading and error bars indicate the standard deviations for the ensemble members in the Δai- and Δai+ cases, respectively.

Figure 8. a) Simulated linear trend in sea level pressure (contours), moisture flux at 925 hPa (vectors), and convergence (shaded). The unit of the moisture flux trend is (kg kg^{-1})(m s^{-1}) $decade^{-1}$. b) Simulated linear trend in the lapse rate of the equivalent potential temperature between the surface and σ=0.9. The unit for the lapse rate of the equivalent potential temperature is K/100 m/decade. The values were averaged over all ensemble members.

Atmos. Chem. Phys. Discuss., doi:10.5194/acp-2016-464, 2016
Manuscript under review for journal Atmos. Chem. Phys.
Published: 24 June 2016

Atmospheric Chemistry and Physics
Discussions
Open Access

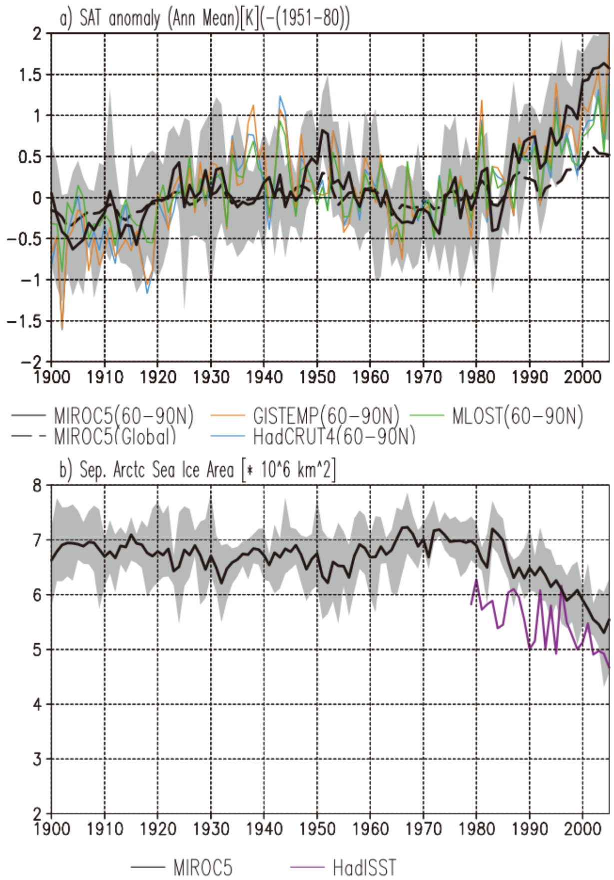

Figure 1. a) Time series of the surface air temperature (SAT) anomaly from the 1951-1980 mean. Solid black, green, orange, and blue lines are the SAT anomalies averaged over 60-90°N in MIROC5's ensemble mean, MLOST, GISTEMP, and HadCRUT4, respectively. The broken black line is the global and ensemble mean SAT anomaly in MIROC5. The gray shaded area indicates the maximum and minimum SAT anomalies between the ensemble members of MIROC5. b) Time series of the September sea ice extent. The black lines represent the ensemble mean. The gray shaded area indicates the maximum and minimum ensemble members. The purple line is the September sea ice extent calculated from HadISST. The units of the SAT anomaly and sea ice extent anomaly are K and 10^6 km^2, respectively.

Atmos. Chem. Phys. Discuss., doi:10.5194/acp-2016-464, 2016
Manuscript under review for journal Atmos. Chem. Phys.
Published: 24 June 2016

Atmospheric Chemistry and Physics
Discussions

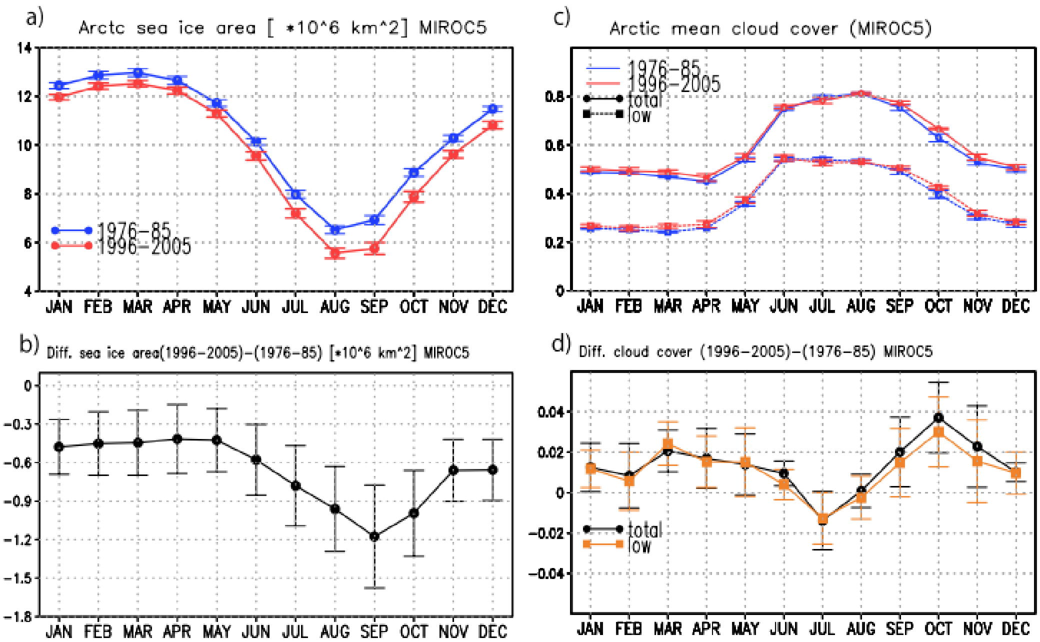

Figure 2. Seasonal cycle of a) Arctic mean sea ice area averaged over the periods 1976-1985 and 1996-2005 in MIROC5 and b) the difference between the means; c) and d) are identical to a) and b) except for the total and low cloud covers. The unit of sea ice area is 10^6 km^2.

Atmos. Chem. Phys. Discuss., doi:10.5194/acp-2016-464, 2016
Manuscript under review for journal Atmos. Chem. Phys.
Published: 24 June 2016

Atmospheric Chemistry and Physics Discussions
Open Access

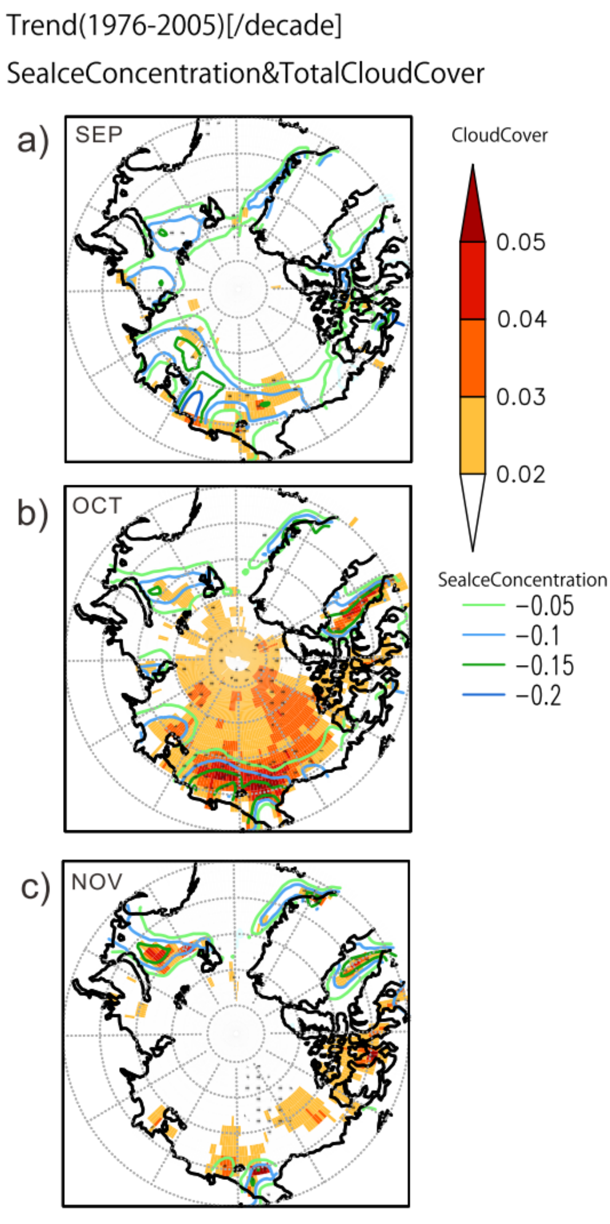

Figure 3. Geographical map of the simulated linear trend in the total cloud cover (shaded) and sea ice concentration (contours) in (a) September, (b) October, and (c) November during the period 1976-2005. The units are decade^{-1}. Dots indicate that the linear trend is not zero at the 95% significance level.

Atmos. Chem. Phys. Discuss., doi:10.5194/acp-2016-464, 2016
Manuscript under review for journal Atmos. Chem. Phys.
Published: 24 June 2016

Atmospheric Chemistry and Physics
Discussions
Open Access

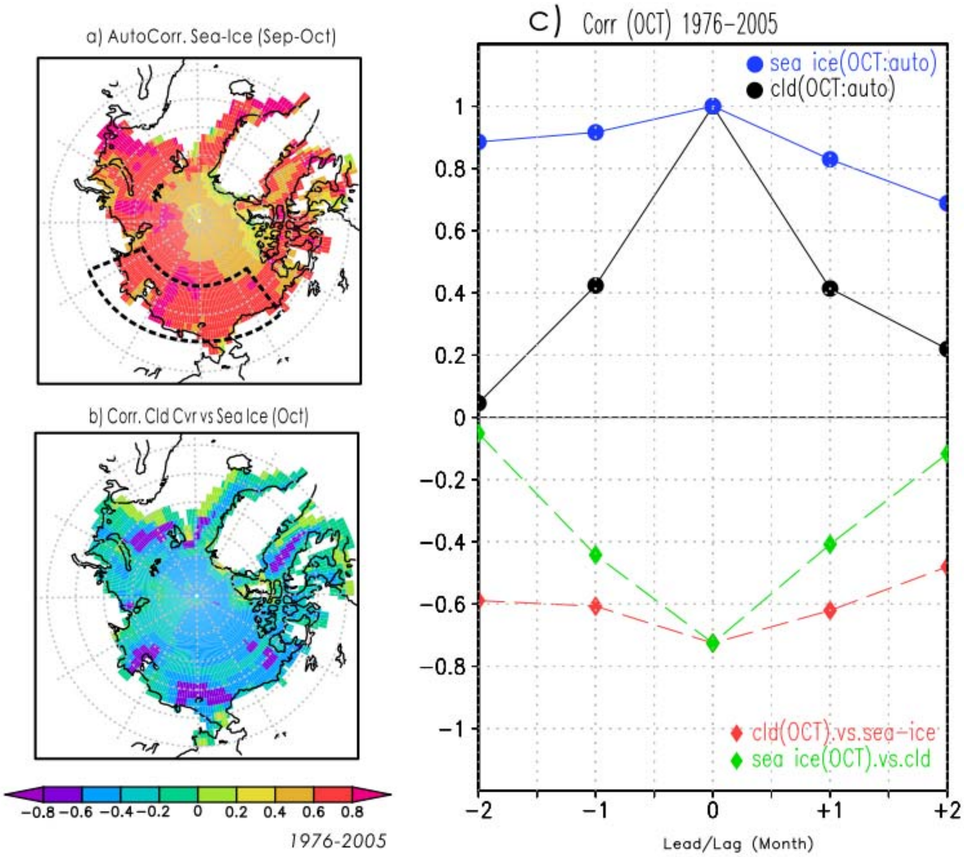

Figure 4. a) Autocorrelation coefficients in the sea ice concentration between September and October in the MIROC5 simulations. b) Correlation coefficients between cloud cover and sea ice concentration in October in the MIROC5 simulations. c) Autocorrelation (closed circles) in the sea ice concentration (blue solid lines) and cloud cover (black solid lines), correlations (closed diamonds) in the lead/lagged sea ice concentrations and October cloud cover (green broken lines), and correlations in the October sea ice concentration and lead/lagged cloud cover (red broken lines) in the MIROC5 simulations. The correlation coefficients were calculated using averages for the boxed region shown in a).

Atmos. Chem. Phys. Discuss., doi:10.5194/acp-2016-464, 2016
Manuscript under review for journal Atmos. Chem. Phys.
Published: 24 June 2016

Atmospheric Chemistry and Physics
Discussions
Open Access

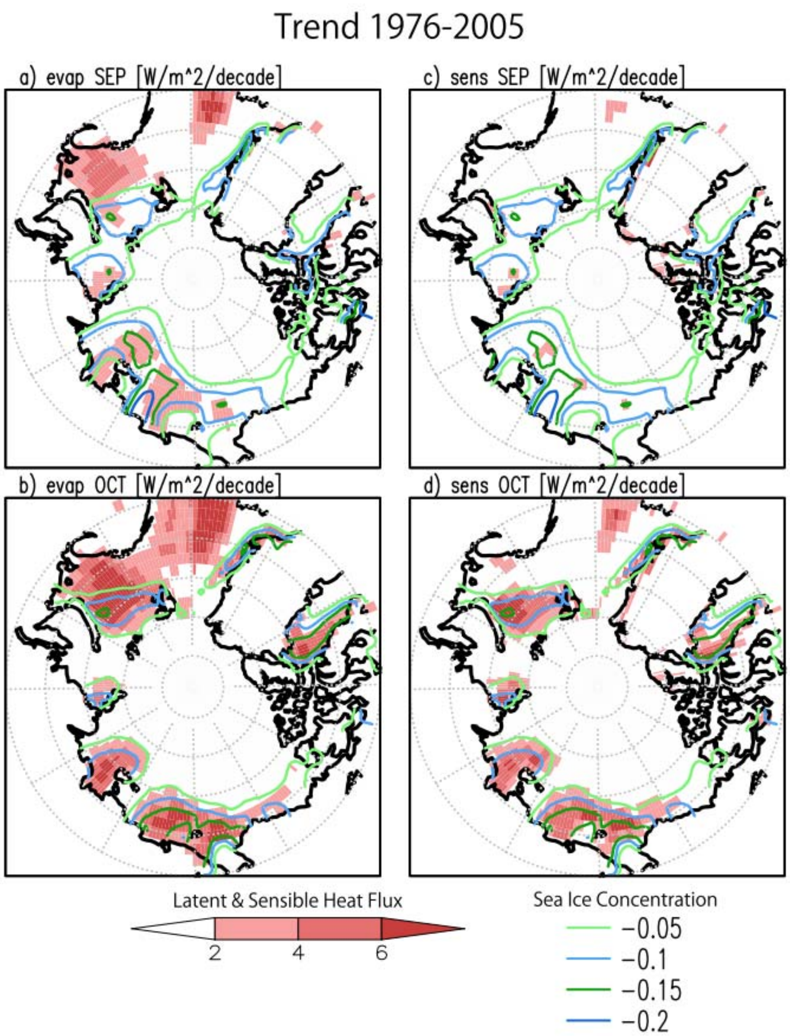

Figure 5. Geographical map of the simulated linear trend in (a, b) latent heat and (c, d) sensible heat fluxes in (a, c) September and (b, d) October during the period 1976-2005. The units are W m^{-2} decade^{-1}. A linear trend for the sea ice concentration (contours) is overlaid, and the units are decade^{-1}.

Atmos. Chem. Phys. Discuss., doi:10.5194/acp-2016-464, 2016
Manuscript under review for journal Atmos. Chem. Phys.
Published: 24 June 2016

Atmospheric Chemistry and Physics
Discussions
Open Access

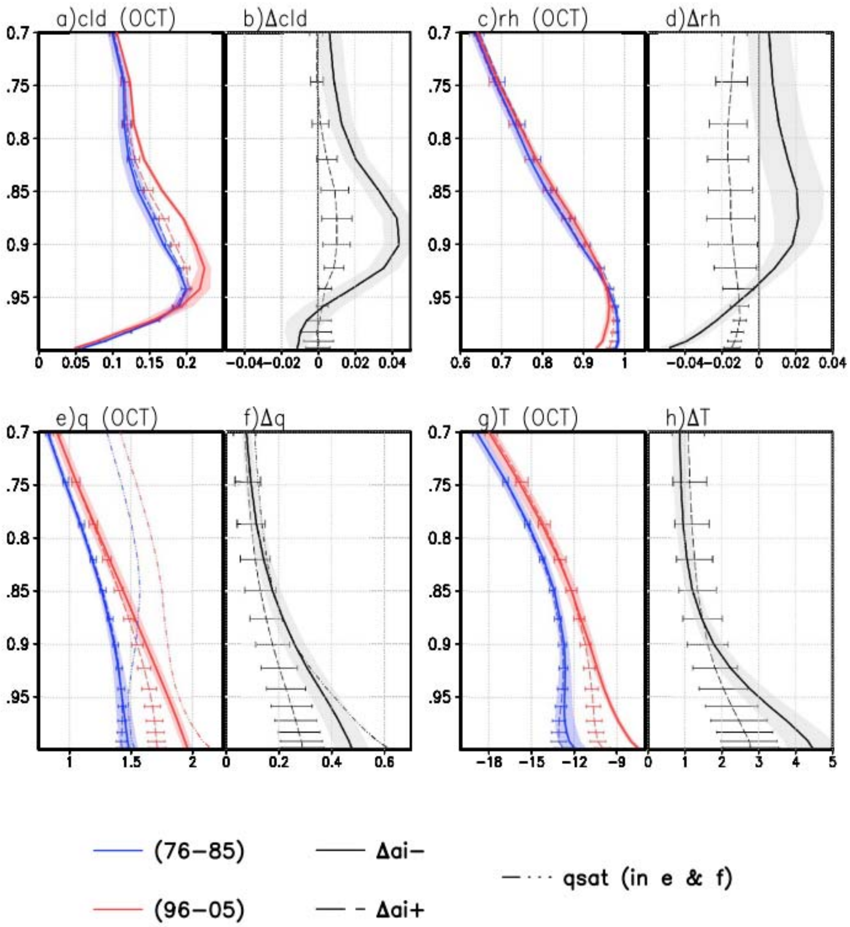

Figure 6. Figure 6. Vertical profiles of the average a) cloud fraction, c) relative humidity, e) specific humidity, and g) air temperature in October in the MIROC5 simulations for the periods 1976-1985 (blue) and 1996-2005 (red). The solid (broken) line represents the Δai- (Δai+) case. See the text for the definitions of the Δai- and Δai+ cases. Vertical profiles of the differences between average b) cloud fraction, d) relative humidity, f) specific humidity, and h) air temperature in October in the MIROC5 simulations for the periods 1976-1985 and 1991-2005. The solid (broken) line represents the Δai- (Δai+) case. The dot-dot-dash lines in e) and f) indicate the saturated specific humidity. The units of air temperature and specific humidity are K

and g kg^{-1}, respectively. Shading and error bars indicate the standard deviations for the ensemble members in the Δai- and Δai+ cases, respectively.

Atmos. Chem. Phys. Discuss., doi:10.5194/acp-2016-464, 2016
Manuscript under review for journal Atmos. Chem. Phys.
Published: 24 June 2016

Atmospheric Chemistry and Physics Discussions
Open Access

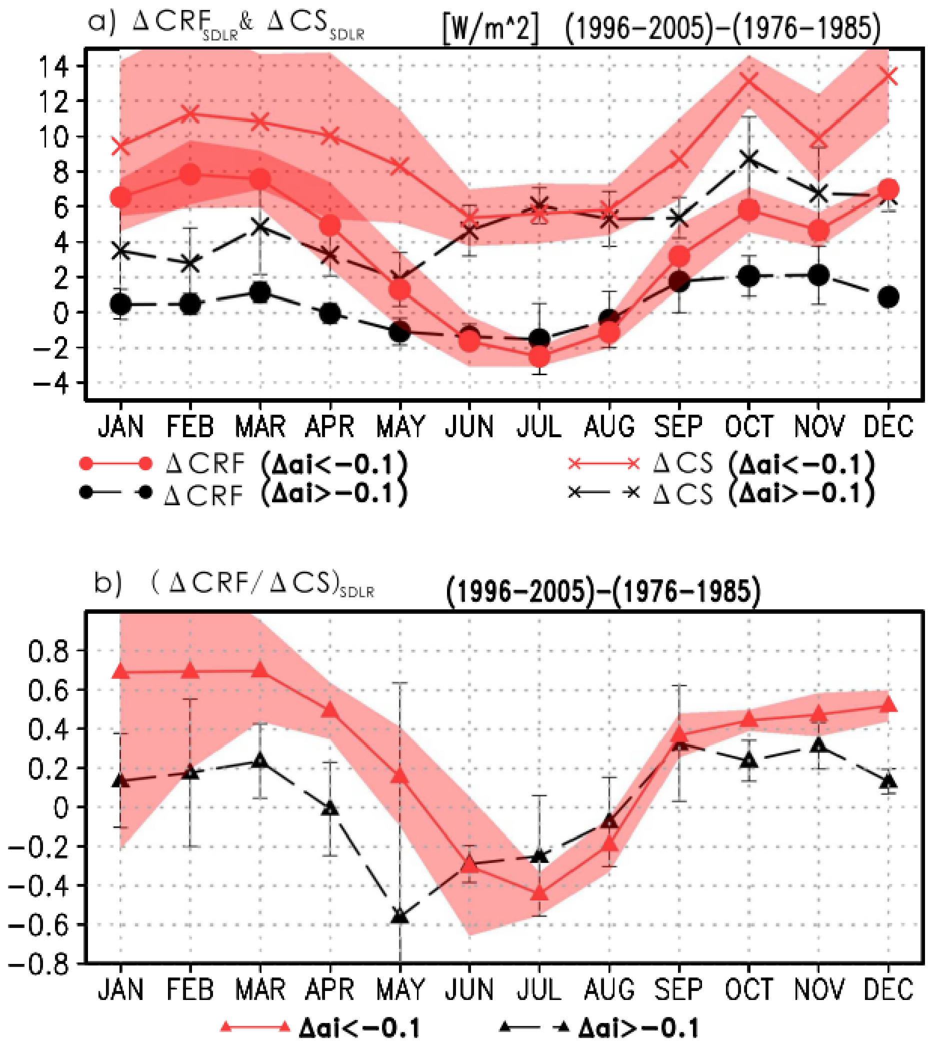

Figure 7. Annual time series of a) the change in (crosses) the CRF in surface DLR (ΔCRF$_{SDLR}$) and (closed circles) clear-sky surface DLR (ΔCS$_{SDLR}$) between the averages for 1976-1985 and 1996-2005 in the MIROC5 simulations and b) (ΔCRF/ΔCS)$_{SDLR}$. The solid red (broken black) lines indicate the Δai- (Δai+) case. See the text for the definition of the index. Shading and error bars indicate the standard deviations for the ensemble members in the Δai- and Δai+ cases, respectively.

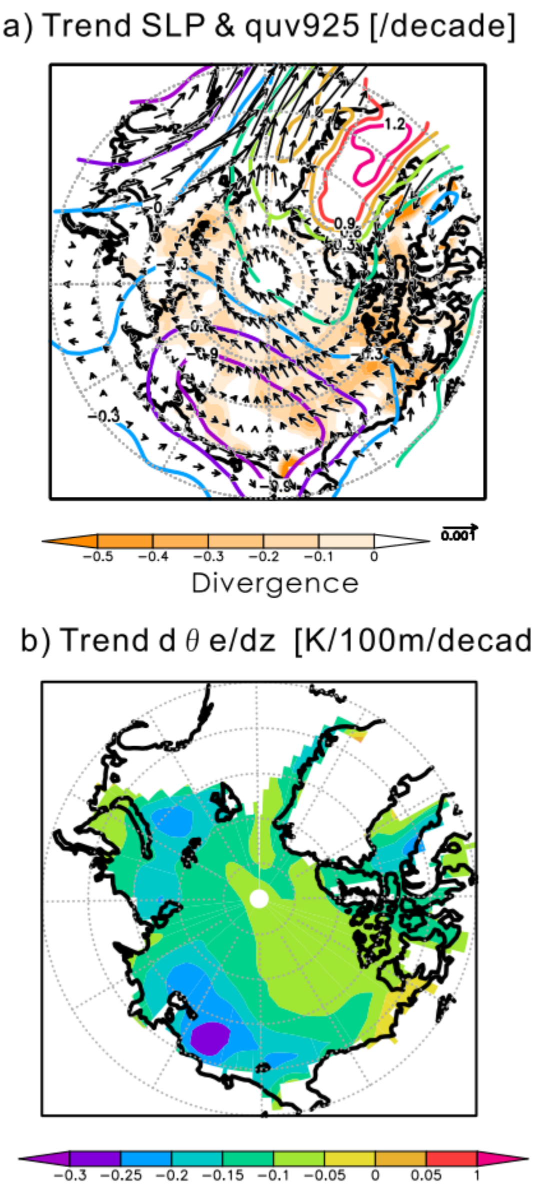

Figure 8. a) Simulated linear trend in sea level pressure (contours), moisture flux at 925 hPa (vectors), and convergence (shaded). The unit of the moisture flux trend is (kg kg^{-1})(m s^{-1}) $decade^{-1}$. b) Simulated linear trend in the lapse rate of the equivalent potential temperature between the surface and σ =0.9. The unit for

Atmos. Chem. Phys. Discuss., doi:10.5194/acp-2016-464, 2016
Manuscript under review for journal Atmos. Chem. Phys.
Published: 24 June 2016

the lapse rate of the equivalent potential temperature is K/100 m/decade. The values were averaged over all ensemble members.

Atmos. Chem. Phys. Discuss., doi:10.5194/acp-2016-464, 2016
Manuscript under review for journal Atmos. Chem. Phys.
Published: 24 June 2016

Table and Figure captions in Appendix

Table A1. Sea surface temperature (SST), sea ice, and other forcing conditions in the sensitivity experiments with MIROC5-AGCM. Other forcings include land use, greenhouse gas concentrations, aerosol emissions, and total solar irradiance. Data in the 1980s indicate an average over the period 1976-1985, and the data in the 2000s combine data for the 1980s and changes for the following 20 years, which were estimated using the linear trend from 1976 to 2005 in the historical simulations.

Figure A1. Seasonal cycle of a) Arctic total cloud cover in each sensitivity simulation using MIROC5-AGCM and b) the difference from the control experiment.

Figure A2. Geographical map of the total cloud cover (shaded) and sea ice concentration (contours) in October in the sensitivity experiments and the differences between experiments.

Atmos. Chem. Phys. Discuss., doi:10.5194/acp-2016-464, 2016
Manuscript under review for journal Atmos. Chem. Phys.
Published: 24 June 2016

Atmospheric Chemistry and Physics Discussions
Open Access
EGU

Table A1. Sea surface temperature (SST), sea ice, and other forcing conditions in the sensitivity experiments with MIROC5-AGCM. Other forcings include land use, greenhouse gas concentrations, aerosol emissions, and total solar irradiance. Data in the 1980s indicate an average over the period 1976-1985, and the data in the 2000s combine data for the 1980s and changes for the following 20 years, which were estimated using the linear trend from 1976 to 2005 in the historical simulations.

Exp. Name	**Sea Ice**	**SST**	**Other**
CTL	**1980s**	**1980s**	**1980**
A2K	**1980s**	**1980s**	**2000**
TA2K	**1980s**	**2000s**	**2000**
IA2K	**2000s**	**1980s**	**2000**
ITA2K	**2000s**	**2000s**	**2000**

Atmos. Chem. Phys. Discuss., doi:10.5194/acp-2016-464, 2016
Manuscript under review for journal Atmos. Chem. Phys.
Published: 24 June 2016

Atmospheric Chemistry and Physics Discussions

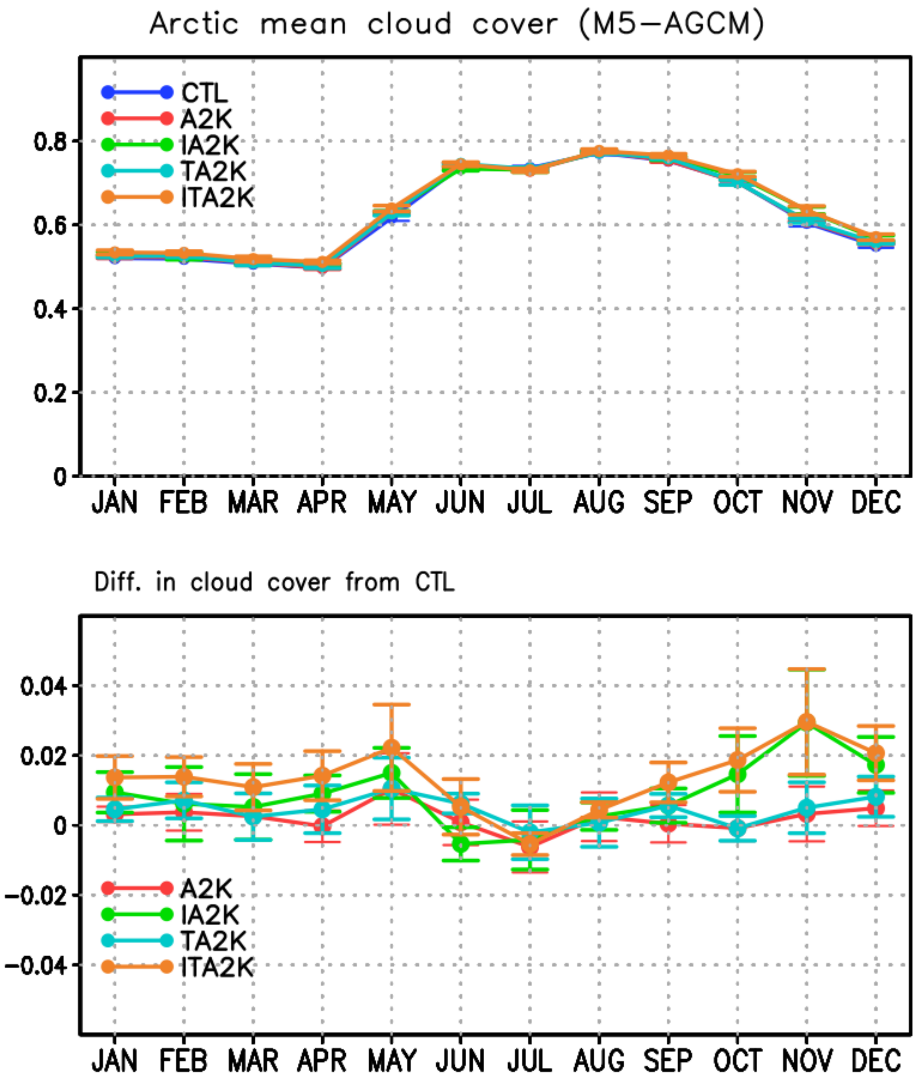

Figure A1. Seasonal cycle of a) Arctic total cloud cover in each sensitivity simulation using MIROC5-AGCM and b) the difference from the control experiment.

Atmos. Chem. Phys. Discuss., doi:10.5194/acp-2016-464, 2016
Manuscript under review for journal Atmos. Chem. Phys.
Published: 24 June 2016

Atmospheric Chemistry and Physics
Discussions
Open Access

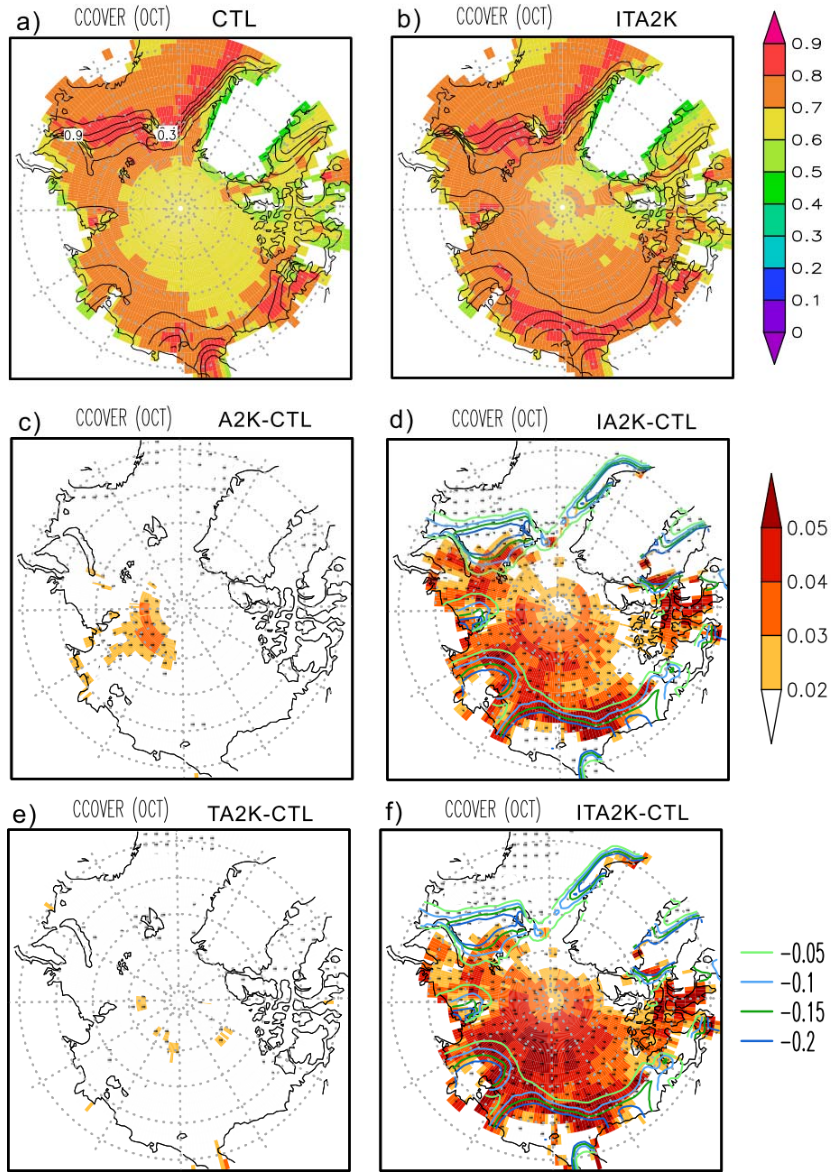

1

2 Figure A2. Geographical map of the total cloud cover (shaded) and sea ice concentration

3 (contours) in October in the sensitivity experiments and the differences between experiments.

4